Journal of Instrumentation

PAPER

Very large SiPM arrays with aggregated output

To cite this article: A. Razeto *et al* 2022 *JINST* **17** P05038

Published by IOP Publishing for Sissa Medialab

Received: *January 17, 2022*
Revised: *March 21, 2022*
Accepted: *April 12, 2022*
Published: *May 25, 2022*

Very large SiPM arrays with aggregated output

A. Razeto,[a,*] **F. Acerbi,**[b,c] **V. Camillo,**[a] **M. Carlini,**[a] **L. Consiglio,**[a] **A. Flammini,**[d] **C. Galbiati,**[e,f] **C. Ghiano,**[a] **A. Gola,**[b,c] **S. Horikawa,**[e] **P. Kachru,**[e] **I. Kochanek,**[a] **K. Kondo,**[a] **G. Korga,**[g,a] **A. Mazzi,**[b,c] **A. Moharana,**[e] **G. Paternoster,**[b,c] **D. Sablone,**[a] **A. Basco,**[h] **V. Bocci,**[i] **W. Bonivento,**[j] **B. Bottino,**[f,k] **A. Caminata,**[k] **S. Copello,**[l,k] **F. Di Capua,**[h,m] **G.K. Giovanetti,**[n] **M. La Commara,**[o,h] **P. Musico,**[k] **E. Paoloni,**[p] **L.P. Rignanese,**[d,q] **S. Sanfilippo,**[r] **C. Savarese,**[f] **Y. Suvorov**[h,m] **and G. Testera**[k]

[a] *INFN Laboratori Nazionali del Gran Sasso, Assergi (AQ) 67100, Italy*
[b] *Fondazione Bruno Kessler, Povo 38123, Italy*
[c] *Trento Institute for Fundamental Physics and Applications, Povo 38123, Italy*
[d] *INFN Bologna, Bologna 40126, Italy*
[e] *Gran Sasso Science Institute, L'Aquila 67100, Italy*
[f] *Physics Department, Princeton University, Princeton, NJ 08544, U.S.A.*
[g] *Department of Physics, Royal Holloway University of London, Egham TW20 0EX, U.K.*
[h] *INFN Napoli, Napoli 80126, Italy*
[i] *INFN Sezione di Roma, Roma 00185, Italy*
[j] *INFN Cagliari, Cagliari 09042, Italy*
[k] *INFN Genova, Genova 16146, Italy*
[l] *Physics Department, Università degli Studi di Genova, Genova 16146, Italy*
[m] *Physics Department, Università degli Studi "Federico II" di Napoli, Napoli 80126, Italy*
[n] *Williams College, Physics Department, Williamstown, MA 01267, U.S.A.*
[o] *Pharmacy Department, Università degli Studi "Federico II" di Napoli, Napoli 80131, Italy*
[p] *Physics Department, Università degli Studi di Pisa, Pisa 56127, Italy*
[q] *Physics Department, Università degli Studi di Bologna, Bologna 40126, Italy*
[r] *INFN Laboratori Nazionali del Sud, Catania 95123, Italy*

E-mail: sarlabb7@lngs.infn.it

[*] Corresponding author.

https://doi.org/10.1088/1748-0221/17/05/P05038

2022 JINST 17 P05038

Abstract: In this work we will document the design and the performances of a SiPM-based photo-detector with a surface area of 100 cm^2 conceived to operate as a replacement for PMTs. The signals from 94 SiPMs are summed up to produce an aggregated output that exhibits in liquid nitrogen a dark count rate (DCR) lower than 100 cps over the entire surface, a signal to noise ratio better than 13, and a timing resolution better than 5.5 ns. The module feeds about 360 mW at 5 V with a dynamic range in excess of 500 photo-electrons on a 100 Ω differential line. The unit can also operate at room temperature, at the cost of an increase of DCR to 10^8 cps.

Keywords: Front-end electronics for detector readout; Large detector systems for particle and astroparticle physics; Photon detectors for UV, visible and IR photons (solid-state); Photon detectors for UV, visible and IR photons (solid-state) (PIN diodes, APDs, Si-PMTs, G-APDs, CCDs, EBCCDs, EMCCDs, CMOS imagers, etc)

ArXiv ePrint: 2201.04615

2022 JINST 17 P05038

Contents

2022 JINST 17 P05038

1 Introduction

Very large scale experiments are being studied or under construction to unlock the fundamental properties of our universe. Experiments such as DUNE, DarkSide, XenonNT, and DARWIN share the requirement of detecting faint pulses of light with many photo-sensors capable of operating in cryogenic environment [1–4].

In the past [5], we demonstrated that it is possible to tile 24 large SiPMs to build a photo-detector working in liquid nitrogen/argon with unprecedented performances. In this work we present a $100 \times 100\,\mathrm{mm}^2$ photo-detector with all the auxiliary electronic components required for installation in a particle detector.

2 SiPMs

In this work NUV-HD-Cryo SiPMs from FBK have been used; these devices represent an evolution from [6] in terms of stability at cryogenic temperature. This allows for higher cell size and lower quenching resistance with respect to the NUV-HD-LF devices used in [5, 7]. An overview of the

SiPM electrical parameters is reported in table 1. The performances of NUV-HD-Cryo SiPMs have been reported in [8–10]: in liquid nitrogen, the Dark Count Rate (DCR) is lower than 1 cps/cm^2 at 9 OV with a negligible after-pulsing probability (<10 %), while the internal cross-talk can reach 50 % at the highest over-voltages.

3 4s6p tile

The peak output current of the NUV-HD-Cryo SiPMs, defined as over-voltage (OV) divided by R_q, is more than three times larger than what was generated in the same condition by the NUV-HD-LF devices, table 1. The higher signal permits the use of a ganging topology that is oriented towards the reduction of the dissipated power at the expense of a lower current at the input of the trans-impedance pre-amplifier.

Table 1. Electrical parameters of the SiPMs and of the assembled tiles in liquid nitrogen. The first section documents the electrical parameters of the single SiPMs: the NUV-HD-LF column refers to the devices studied in [5–7], while the NUV-HD-Cryo are the subject of this work and have been documented in [8–10]. For the breakdown voltage and for the quenching resistance the error term describes the standard deviation of the population, rather than a measurement uncertainty. The second section compares the performances of the assembled tile with the 4×2s3p ganging scheme described in [5], while the third section describes the performance of the new 4s6p ganging scheme described in this work.

Group	**Parameter** at 77 K	**NUV-HD-Cryo**	**NUV-HD-LF**
SiPM	SiPM Size	7.9×11.7 mm^2	
	Cell Unit Size (S_c)	30 µm	25 µm
	Cell Capacitance (C_d)	65 fF	40 fF
	Number of cells (N_c)	100 k	150 k
	Quenching Resistance (R_q)	(3.0 ± 0.3) MΩ	(10 ± 1) MΩ
	Breakdown Voltage (V_{bd})	(27.5 ± 0.3) V	(28.0 ± 0.4) V
	Maximum Over-voltage (OV_{MAX})	9 V	6 V
	Primary Recharge Time ($R_q \times C_d$)	180 ns	400 ns
4×2s3p Tile	Aggregated Recharge Time (τ)	350 ns	≈600 ns
	Current Peak ($I_p = {}^1/_2\, C_d \,/\, \tau$)	100 nA/OV	30 nA/OV
	Input noise density at 1 MHz	18 pA/$\sqrt{\mathrm{Hz}}$	15 pA/$\sqrt{\mathrm{Hz}}$
	SNR with Matched Filter	4/OV	4/OV
4s6p Tile	Aggregated Recharge Time (τ^+)	350 ns	
	Current Peak ($I_p = {}^1/_4\, C_d \,/\, \tau$)	50 nA/OV	
	Input noise density at 1 MHz	9 pA/$\sqrt{\mathrm{Hz}}$	
	SNR with Matched Filter	>3.8/OV	

2022 JINST 17 P05038

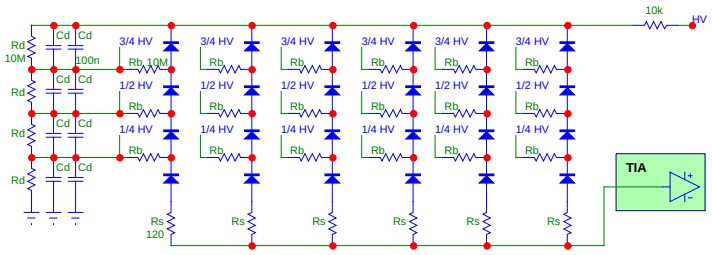

(a) 4s6p Tile.

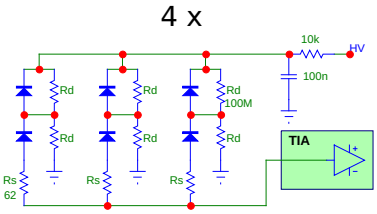

(b) 2s3p Quadrant.

Figure 1. Schematics of the *4s6p* SiPM layout: six branches of four SiPMs are connected with a single TIA pre-amplifier for a total of 24 sensors. As a reference, one quadrant of the *4×2s3p* tile is shown: the readout of 24 SiPMs is achieved by summing four identical stages with an active adder (not shown).

3.1 SiPM connection scheme

Figure 1 depicts the *4s6p* topology where six branches each with four SiPMs are fed to a single TIA. In [5] we used four quadrants each with an individual TIA to read 24 SiPMs: each quadrant was configured with a *2s3p* layout (three parallel branches of two SiPMs in series) and an active summing node was required to aggregate the signal from the four TIAs.

The *4s6p* configuration drastically simplifies the scenario: only one pre-amplifier is required without other circuit elements. However, the stronger ganging reduces the signal by a factor two with respect to the *2s3p* scenario. This happens because the capacitive coupling of the SiPMs in series attenuates the photo-current by the series order (4 in this case). The next section will demonstrate the possibility to maintain nearly the same signal to noise ratio as that of the *4×2s3p* configuration. This is achieved by reducing the input noise of the TIA with a proper selection of the circuit elements.

3.2 Divider

A precision voltage divider is required to provide an even voltage bias distribution to all the devices. At cryogenic temperature, the DCR-induced current is in sub-picoampere, a region that is sensitive to surface leakages of the SiPMs or from the PCB.[1] The passive divider, shown in figure 1, is provided by four resistors. The accuracy of the bias distribution affects the quality of the signal. Assuming the operation at 7 OV in liquid nitrogen, a disuniformity of 1 % in the resistor leads to an over-voltage spread of 5 %. This is reflected in the form of an equivalent variation of the gain between different SiPMs in the same tile. The value of R_d defines the stability of the divider for current leakages of the SiPMs or of the PCBs: with R_d=10 MΩ a SiPM surface leakage of 50 nA (over 30 V) would affect the divider by less than 1 %.

For the choice of R_d, Vishay resistors MCT06030C1005FP500 have been selected as they provide a ±1 % tolerance with very low temperature drift. Eight 100 nF PEN capacitors (Panasonic ECW-U1104V33) are placed in parallel to the divider. The capacitors and the 10 kΩ resistor form a filter for the noise coming from the bias line. The branch resistors R_b decouple the SiPMs from

[1] Inpurities on the surface of the SiPM (or on the PCB) can lead to surface leakage. At room temperature its contribution is negligible with respect to the dark rate of the SiPM (few pA versus nA/mm^2). At cryogenic temperature the current trough the junction drops by more than 6 orders of magnitude, below the surface leakage.

2022 JINST 17 P05038

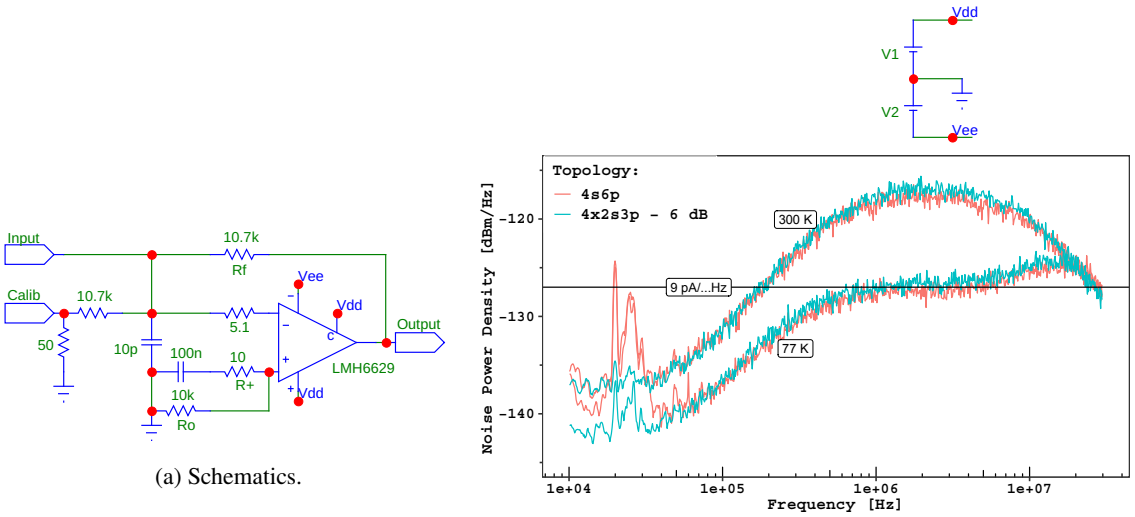

(a) Schematics.

(b) Output noise spectra.

Figure 2. Trans-impedance amplifier schematics and noise performances. The output noise density is reported at room temperature and in liquid nitrogen for the same tile configured as *4s6p* (red) and as *4×2s3p* (blue). The noise of the latter has been scaled by −6 dB to simplify the comparison. The horizontal line represents the noise predicted by equation (3.2) at 1 MHz for the *4s6p* topology: an agreement better than few percent between the data and the model is achieved. The spurious noise at about 25 kHz is due to the specific setup that can be configured in both ganging topologies; it is not present in dedicated *4s6p* circuits.

each other and from the divider capacitors, thus eliminating unwanted paths to the signal. For convenience, same Vishay part for the branch resistors and for the divider resistors were used.

3.3 TIA

We used the trans-impedance amplifier (TIA) described in [7] that is based on the LMH6629 from Texas Instruments operating from 60 K to 300 K. The chip exhibits a voltage input noise equivalent to a R_{TIA}=20 Ω resistor and an input current noise (I_{TIA}) that is below 1 pA/$\sqrt{\text{Hz}}$ for temperatures lower than 200 K. The TIA is configured with a gain of 10.7 kΩ with disabled compensation and without any feedback capacitor, see figure 2a.

The impedance of each branch with S SiPM in series is defined as the sum of the series resistance R_s (62 Ω or 120 Ω for *4×2s3p* and *4s6p*, figure 1) and the electrical components of the SiPMs from table 1 (N_c is the number of cells, R_q is the value of the quenching resistor and C_d the capacitance of the cell). Using a simplified notation:[2]

$$\mathcal{Z}_{\text{branch}} = R_s + (S/N_c \times R_q) \,||\, Z(C_q \,/\, S/N_c) + Z(C_d \,/\, S/N_c)) \tag{3.1}$$

where C_q is the parasitic capacitance of the quenching resistor (typically 1/10 C_d). Two poles/zeros can be identified $\mathcal{P}_l = C_d(R_q + N_c/S \times R_s)$ ≃400 kHz and $\mathcal{P}_h = C_q R_q$ ≃8 MHz.

For a generic tile configured with Q quadrants each with P parallel branches each of S SiPMs in series, the total input noise of the TIA in liquid nitrogen at 1 MHz can be calculated with the following formula:

$$I_n\{1\text{Mhz}\} = \sqrt{\frac{Q \times 4k_B T}{(R_s + S/N_c \times R_q)/P + R_{\text{TIA}}} + 2e^- \times Q \times I_{\text{TIA}}} \tag{3.2}$$

[2] $a||b = (a^{-1} + b^{-1})^{-1}$ and $Z(C) = 1/sC$ (as in [11]).

2022 JINST 17 P05038

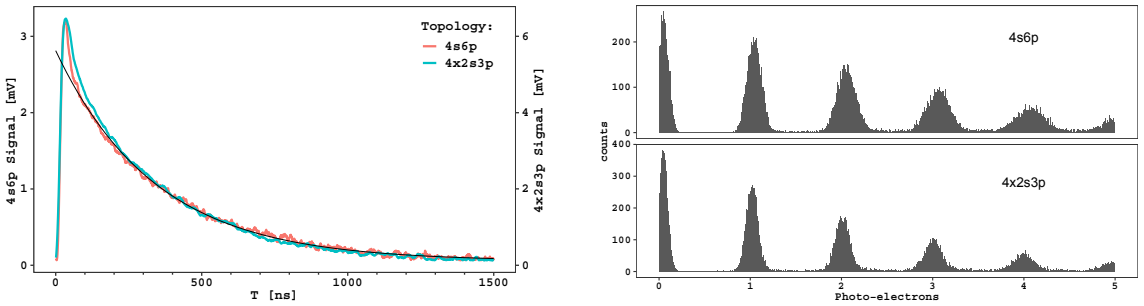

(a) Signal shape.

(b) Pulse spectrum.

Figure 3. Average signal for the first photo-electron of the *4s6p* and of the *4×2s3p* (scaled by 0.5) topologies in liquid nitrogen at 6.5 OV (left). The *4s6p* signal is described as an exponential with τ=(350 ± 1) ns at better than 50 µV after the first 50 ns (black line). The pulse spectrum for the signal integral (on 3 τ) is reported (right). For both the configurations, SNR larger than 35 is achieved over a gain of each SiPM of 2.7×10^6 electrons.

where the adder noise (if needed) is neglected. At 1 MHz $\mathcal{P}_l$ affects $\mathcal{Z}_{\text{branch}}$ by less than 15 %. Therefore we can approximate the circuit as an inverting amplifier (and consequently equation (3.2)). At lower frequencies, the noise gain is reduced by the presence of the pole $\mathcal{P}_l$ and only the I_{TIA} becomes relevant. At higher frequencies the parasitic capacitance of the quenching resistor comes into play (pole $\mathcal{P}_h$) leading to an increased noise gain, until the cut-off from amplifier bandwidth. Figure 2b reports the output noise spectra measured on the same SiPM tile configured in *4×2s3p* and *4s6p*; the agreement with the model is very good.

At room temperature R_q, is smaller by a factor 2 to 3 respect to its value at 77 K and the Johnson noise increases with the square root of the temperature. Both result in a noise density higher than the cryogenic counterpart. Moreover the gain bandwidth product (GBP) of the LMH6629 is one fourth respect to the GBP at cryogenic configuration [7]. Therefore, the cut-off happens within the noise gain plateau and spectra does not show any features.

3.4 Pulse shape and SNR

As described in [11], the recharge part of the signal of SiPMs includes two exponential components (τ_i and τ_d). The authors focused on small SiPMs, for which $R_q C_d \gg N_c R_s (Cd||Cq)$. This leads to the assumption $\tau_i \ll \tau_d$. For 1 cm^2 large devices, such assumption breaks and it is necessary to solve the equations with ganged SiPMs. The value of R_s=120 Ω at 77 K leads to the degeneration of the two components, resulting in a pure exponential recharge after the first 50 ns, figure 3a.

Concurrently with R_s=120 Ω, the input noise of the *4s6p* tile is halved with respect to the noise of the *4×2s3p* and R_s=60 Ω, as shown in figure 2b. Similarly, the signal amplitude for the *4s6p* is halved, as discussed in the caption of figure 3a. Since the signal shape and the noise bandwidth remain unaltered (as result of the identical noise gain), the signal to noise ratio (SNR) is preserved. The SNR is calculated as the gain of the system divided by its average baseline noise (in the pre-trigger window). Figure 3b reports the pulse spectrum for the same tile acquired in both configurations.

The SNR depends on the filtering: at 6.5 OV for raw data the SNR is about 5.5 and for the integrated wave-forms more than 35 is achieved. The integration correspond to a low pass filter

2022 JINST 17 P05038

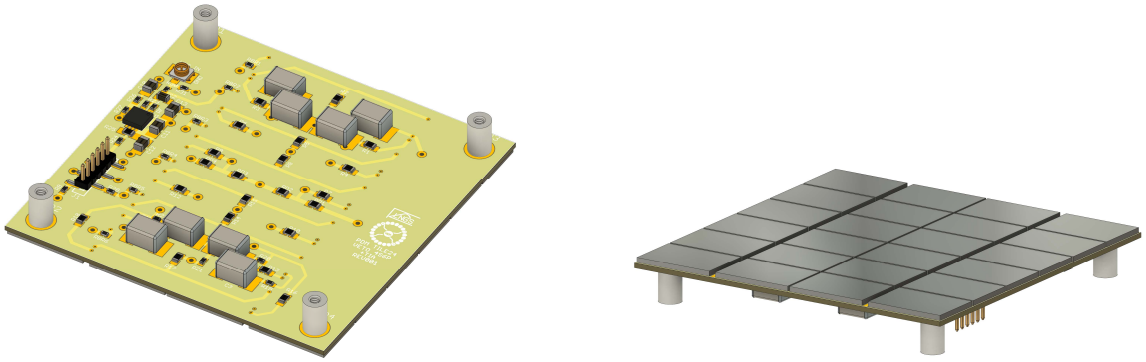

Figure 4. Tile+ drawings: the 10 pF capacitor is buried in the PCB. The calibration input, provided by the miniaturized U.FL connector, is useful to test at cryogenic temperature the circuit before bonding the SiPMs.

with frequency cut at about 400 kHz. It is interesting to evaluate the SNR for other types of filtering: from the matched filter theory [12], the optimal signal is achieved by the convolution of the wave-forms with the reference shape, figure 3a. The result is a cusp-like signal ($e^{-|t|/\tau}$), whose maximum amplitude is used to estimate the charge of the event. Alternatively, the wave-forms can be filtered by the correlation with the reference shape, obtaining a *critically damped*-like signal ($te^{-t/\tau}\ \forall\, t > 0$). At 6.5 OV the SNR obtained for the two options is respectively 28 and 21, with the same noise bandwidth (450 kHz). The time of the maximum for the matched filtered wave-forms provides accurate timing of the pulse, with a resolution of about 3 ns at 6.5 OV.

3.5 Uniformity

The uniformity of gain between the 24 SiPMs can be evaluated by the spread of the first photo-electron peak with laser illumination. In the setup the laser photons were uniformly distributed on the surface of the tile with an average number of detected photo-electrons below 50 %. It is safe to assume that in average all the SiPMs contributed to the first photo-electron peak, which has a resolution of (8 ± 1) % (1σ) for both topologies. The resolution accounts for the electronic noise and the dispersion of the gain (and pulse shape). The uniformity of the gain can be calculated to be (7 ± 1) % over all the SiPMs of the tested tile. This value is in agreement with the spread predicted by the divider uniformity, section 3.2, that accounts for 5 %.

4 Tile+

A Tile+ is a single unit including 24 SiPMs (top layer) and the required readout electronics (bottom layer). The *4s6p* ganging scheme described earlier is used, therefore only one TIA is needed. Figure 4 depicts the Tile+. The signal output, the HV bias, the ground and the low voltages (±2.5 V) are routed on pin strip connector (M50-3630642 from Harwin).

Four threaded 5 mm spacers (97730506330R from Wurth) are soldered to the PCB during the automatic population of bottom components in the first stage of the assembly. A low temperature Tin-Bismuth alloy is used to avoid damaging the PEN capacitors which, after reflow at high temperatures, tend to produce leakage in cryogenic environment.

2022 JINST 17 P05038

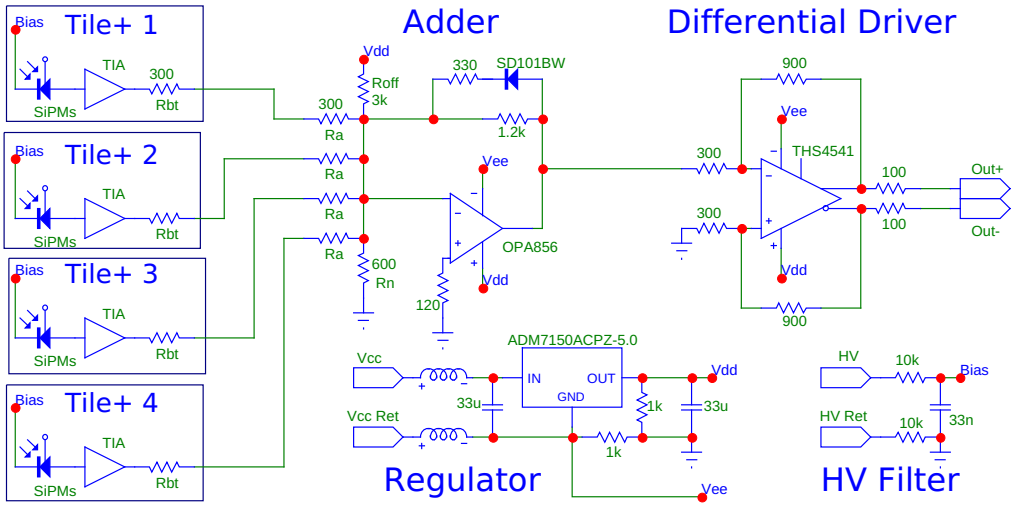

Figure 5. Schematics of the MB1/4.

After the validation of the electrical circuit in liquid nitrogen, the SiPMs are placed on the PCB using a Westbond 7200CR manual die bonder. We use an Indium-Tin solder (Indium Corp Indalloy#1E), dispensed automatically in six 300 µm dots by an Auger valve installed on a fluid dispenser robot [13]. As final step, the tile is processed again in the reflow oven with a thermal profile compatible with the bottom components. The PCB finish and the SiPM backside are in gold. This provides good adhesion and avoids the formation of weak inter-metallic compounds with indium.

The dimension of the PCB is $49.5 \times 49.5\,\mathrm{mm}^2$ with a fill factor of 90 %. The PCB is realized in Arlon 55NT that exhibits low thermal shrinkage 6 ppm/K to 9 ppm/K. This is necessary to avoid stress on the silicon that has a shrinkage of about 2.5 ppm/K [14].

In liquid nitrogen the Tile+ dissipates a power of 50 mW with an output swing of 1.7 V (before back-termination), corresponding to about 450 photo-electrons at 7 OV. The performances in terms of SNR, signal shape and pulse spectrum remain unaltered with respect to what is shown in the previous section.

5 MB1/4

Given the very high SNR for the Tile+, it is possible to aggregate four tiles in a single analog photo-detector with a total surface of $100\,\mathrm{cm}^2$. The schematics of such device, called *MB*1/4, is shown in figure 5. The finished unit is shown in figure 7 and in figure 9.

5.1 Adder

The aggregation of the four Tile+ is performed by an analog adder with double gain. This circuit is based on a OPA856 from Texas Instruments, capable of working in liquid nitrogen with a gain bandwidth product of about 800 MHz, with a dissipation of 50 mW on a power rail of 5 V. At cryogenic temperature the peak to peak output swing is limited to 2.4 V: to maximise the dynamic range for unipolar (positive) pulses, the output is biased at −1 V by the R_{off} resistor, leaving a useful swing of 2.2 V. The small signals gain is 2 V/V, as defined by $R_f/(R_a+R_{bt})$. The optional Schottky

2022 JINST 17 P05038

diode (SD101BW) provides a second gain of 0.44 V/V for large pulses. In liquid nitrogen and assuming an over-voltage of 7 V, without the diode the dynamic range is about 300 photo-electrons, that becomes 500 for the configuration with double gain, see figure 6a. The bandwidth of the adder at 77 K exceeds 80 MHz and therefore does not affect the pulse shape (the TIA is limited to 30 MHz). Figure 6b reports the input noise equivalent for the adder: the comparison term is the output noise of the TIA, figure 2b, incremented by 6 dB.

5.2 Differential driver

A high dynamic range cryogenic fully differential transmitter has been developed to facilitate scaling up to many photo-detectors in a ground isolated environment (see later). The differential transmitter is based on a THS4541 from Texas Instruments. In liquid nitrogen, the chip is capable of driving low impedances (50 Ω to 100 Ω transmission lines) with a large output swing (about 7.4 V differential) with a supply of 5 V and a power consumption of 70 mW. To match the output swing of the adder (2.2 V), a gain of 3 V/V per branch is used. Considering the loss of the single-ended to differential conversion (a factor 1/2), the amplitude of the single photo-electron becomes 10.5 mV before the backside termination (5 mV on the cable), which is well above the typical noise of a differential line for the 30 MHz bandwidth. Since the rise-time (10-90 %) of the transmitter with 10 m of cable is below 4 ns and its input noise density is in the order of −160 dBm, the effects on the signal quality are negligible.

5.3 Voltage regulator

In the Tile+ and in the MB1/4, the op-amps are configured as inverting amplifiers. Therefore, all the currents (input and output) sum to zero. As a consequence, it is feasible to create a local ground with a simple voltage divider (and proper bypass capacitors). The main advantage of this design due to

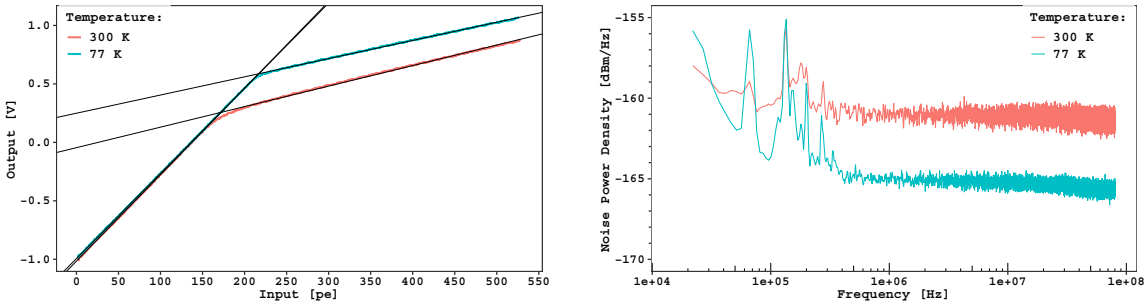

(a) Dynamic range.

(b) Input noise.

Figure 6. Perfomances of the OPA856-based adder in liquid nitrogen and at room temperature. For the dynamic range we assume the amplitude of the photo-electron at 3.5 mV. The SD101BW was selected for its low intervention threshold and small distortions at 77 K. Up to the first 150 photo-electrons the diode is reverse biased and the system is perfectly linear. The input noise spectra of the adder accounts for the noise gain (10) of the described configuration. Therefore, the right comparison is not with the output noise density of a single TIA, but with the four channels summed (figure 2b scaled by $\sqrt{4}$). The increase of the 1/f noise at cryogenic temperature is typical in the FET-based electronics and becomes relevant only for integration times larger than 0.5 ms.

2022 JINST 17 P05038

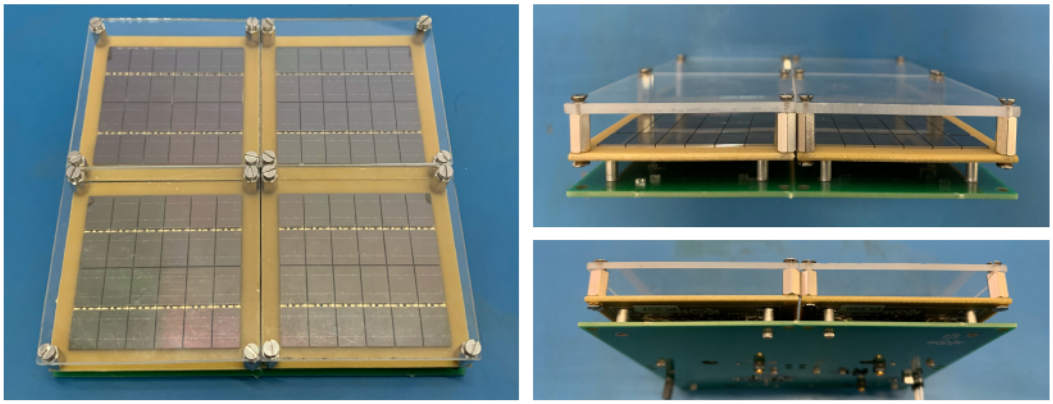

Figure 7. Populated MB1/4: this version has 5 mm frame around each Tile+ to simplify the manipulation and to hold an acrylic protection window. The frame-less version has a fill factor of 88 % (dimensions $100 \times 100 \times 7\,\mathrm{mm}^3$), while this version is at about 60 % ($120 \times 120 \times 15\,\mathrm{mm}^3$ with the protection). The PCB of the MB1/4 is not critical and either FR4 (as here) or Arlon 55NT can be used.

the differential transmission, is that it keeps the local ground isolated from the receiver electronics and from the cryostat, which reduces ground loops and noise injection. To further reduce noise and ripple from the power supply, a low drop voltage regulator (LDO) to the system is added. The ADM7150ACPZ-5.0 from Analog Devices provides a protection from the accidental fluctuations of the power supply up to 12 V, works in liquid nitrogen with noise density in the range of −160 dBm to −165 dBm and a drop of the order of 0.5 V. Therefore, the minimum power consumption of the fully instrumented MB1/4 is 65 mA x 5.5 V.

5.4 Connections

The MB1/4 can be connected with standard unshielded RJ45/U. Categories above 5e satify the bandwidth and the FEP jacket is compatible with cryogenic environment. At room temperature, two isolated power supplies are required. A Keysight 3649A for the low voltage, and a Keithley

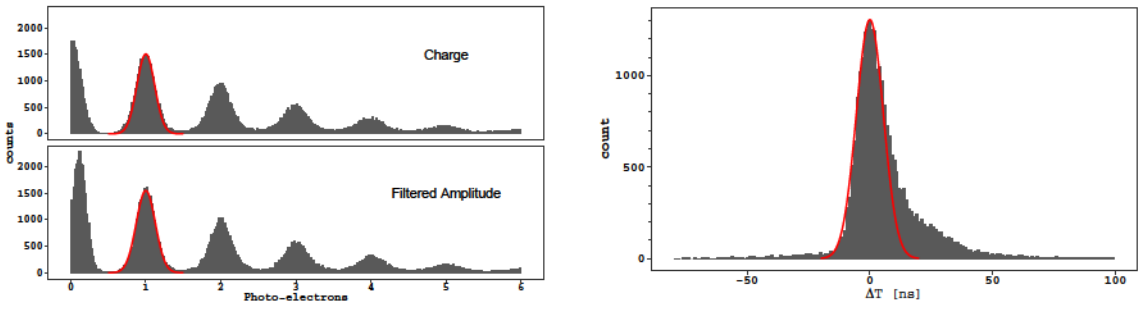

(a) Pulse Spectrum.

(b) Timing.

Figure 8. Performances of the MB1/4 at 7 OV in liquid nitrogen. The finger plots for both charge and filtered amplitude (see text for details of filtering) exhibit similar SNR, 16 ± 1 versus 13.0 ± 0.5. The resolution of the first photo-electron is (12.5 ± 0.5) % for both algorithms. On the other hand, with the filtered signal it is possible to measure the time of the photo-electrons (relative to the laser pulse) achieving a jitter of 5.5 ns. The asymmetric shape of the time jitter is due to the presence of after-pulses in the signal.

2022 JINST 17 P05038

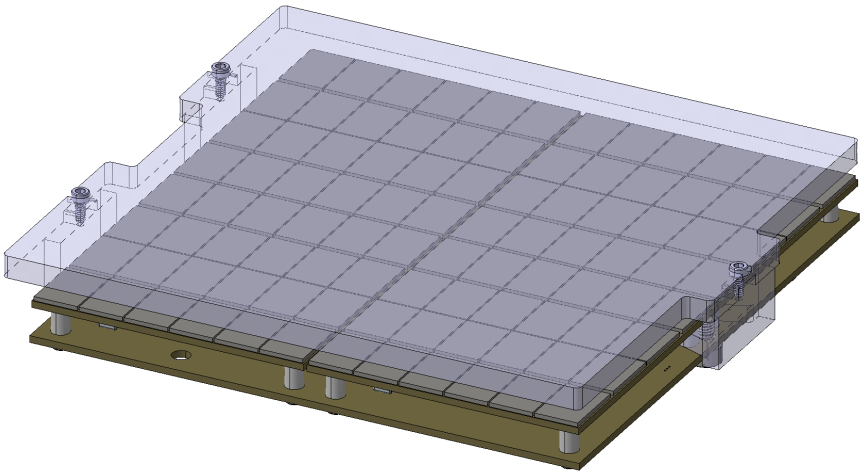

Figure 9. Rendering of the MB1/4 with an external acrylic protection in a border-less configuration. With this design it is possible to install several MB1/4 on an optical plane with only 5 mm of spacing for a total fill factor of 84 %.

2450 SMU for the HV bias have been used for this purpose. The HV is internally filtered in the MB1/4 with a π circuit, that protects the local ground from noise injection.

The signal is delivered to a simple differential receiver implemented with a LMH6552 from Texas Instruments that matches the high dynamic range and low noise requirements. To limit the power dissipation due to the −1.5 V of baseline on the termination, an AC coupling on the receiver is required. Standard 100 µF ceramic capacitors with the 100 Ω termination resistor provide a pole well outside the region of interest.

5.5 Performances

Figure 8a reports the pulse spectrum of the charge (in a 3 τ window) and of the matched-filtered amplitude, section 3.4. The timing of the single photo-electron (from the location of the maximum of the filtered signal) is shown in figure 8b: a jitter of 5.5 ns is achieved.

The SNR for both charge and filtered signal is above 13 and the resolution of the first photo-electron is around 12 %. The gain spread for all 96 SiPMs, once subtracted the baseline noise as discussed in section 3.5, is about 10 %.

6 Conclusions

In this work, the design and the implementation of a very large SiPM array for cryogenic application has been documented. An SNR larger than 13 with a resolution of the first photo-electron 12.5 % was demonstrated. This is for a photo-detector that includes 96 x 1 cm^2 SiPMs. The timing resolution of this array is 5.5 ns, a value better than several PMTs of the same size. The dynamic range exceeds 500 photo-electrons with a power dissipation of 360 mW. The operation of this unit requires standard laboratory power supplies and simple differential receiver.

2022 JINST 17 P05038

Acknowledgments

We acknowledge support from the Istituto Nazionale di Fisica Nucleare (Italy) and Laboratori Nazionali del Gran Sasso (Italy) of INFN, from NSF (US, Grant PHY-1622415 and PHY-1812540 for Princeton University), from the Royal Society U.K. and the Science and Technology Facilities Council (STFC), part of the United Kingdom Research.

References

[1] DUNE collaboration, *Prospects for beyond the Standard Model physics searches at the Deep Underground Neutrino Experiment*, *Eur. Phys. J. C* **81** (2021) 322 [arXiv:2008.12769].

[2] DarkSide-20k collaboration, *DarkSide-20k: a 20 tonne two-phase LAr TPC for direct dark matter detection at LNGS*, *Eur. Phys. J. Plus* **133** (2018) 131 [arXiv:1707.08145].

[3] XENON collaboration, *Projected WIMP sensitivity of the XENONnT dark matter experiment*, *JCAP* **11** (2020) 031 [arXiv:2007.08796].

[4] DARWIN collaboration, *DARWIN: towards the ultimate dark matter detector*, *JCAP* **11** (2016) 017 [arXiv:1606.07001].

[5] M. D'Incecco et al., *Development of a novel single-channel, 24 cm^2, SiPM-based, cryogenic photodetector*, *IEEE Trans. Nucl. Sci.* **65** (2018) 591.

[6] F. Acerbi et al., *Cryogenic characterization of FBK HD near-UV sensitive SiPMs*, *IEEE Trans. Electron Devices* **64** (2017) 521.

[7] M. D'Incecco et al., *Development of a very low-noise cryogenic preamplifier for large-area SiPM devices*, *IEEE Trans. Nucl. Sci.* **65** (2018) 1005.

[8] A. Gola et al., *NUV-sensitive silicon photomultiplier technologies developed at Fondazione Bruno Kessler*, *Sensors* **19** (2019) 308.

[9] M.G. Boulay et al., *Direct comparison of PEN and TPB wavelength shifters in a liquid argon detector*, *Eur. Phys. J. C* **81** (2021) 1099 [arXiv:2106.15506].

[10] M.G. Boulay et al., *SiPM cross-talk in liquid argon detectors*, arXiv:2201.01632.

[11] D. Marano et al., *Silicon photomultipliers electrical model extensive analytical analysis*, *IEEE Trans. Nucl. Sci.* **61** (2014) 23.

[12] G. Turin, *An introduction to matched filters*, *IEEE Trans. Inform. Theory* **6** (1960) 311.

[13] I. Kochanek, *Packaging strategies for large SiPM-based cryogenic photo-detectors*, *Nucl. Instrum. Meth. A* **980** (2020) 164487.

[14] I. Kochanek, *SiPMs for cryogenic temperature*, *Nuovo Cim. C* **42** (2019) 62 [arXiv:1904.00949].